ACS APPLIED MATERIALS & INTERFACES

RESEARCH ARTICLE

www.acsami.org

Mechanism of Recombination Losses in Bulk Heterojunction P3HT:PCBM Solar Cells Studied Using Intensity Modulated Photocurrent Spectroscopy

Joshua C. Byers,[†] Scott Ballantyne,[‡] Konstantin Rodionov,[‡] Alex Mann,[‡] and O. A. Semenikhin*[,†]

[†]Department of Chemistry, The University of Western Ontario, London, Ontario N6A 5B7, Canada

[‡]Wired Sun Inc., 112 College Street, Toronto, Ontario, M5G 1L6, Canada

ABSTRACT: Intensity modulated photocurrent (IMPS) and photovoltage (IMVS) spectroscopies were used to study the mechanism of photoprocesses in P3HT:PCBM bulk heterojunction organic solar cells at various light intensities. The use of the frequency domain techniques allowed us to separate the bulk and interfacial processes and gain a valuable insight into the mechanism of losses in these devices. The results provide direct evidence that interfacial nongeminate recombination is one of the dominant loss and aging mechanisms in bulk heterojunction organic solar cells. The trapping of photoexcited holes in the P3HT phase was found to contribute to the increased recombination rate. The results suggest that promising ways of improving the efficiency of bulk heterojunction solar cells may be reducing the charge trapping both at and near the P3HT:PCBM interface, as well as improving the efficiency of charge extraction at contacts.

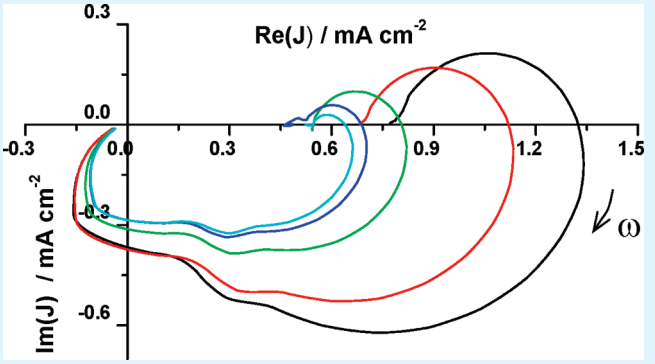

KEYWORDS: intensity modulated photocurrent spectroscopy (IMPS), P3HT:PCBM organic solar cells, organic photovoltaics, organic solar cells, bulk heterojunction, surface and interfacial recombination

1. INTRODUCTION

Despite impressive improvements over the past 10 years, the efficiency and the service life of organic solar cells still remain too low for them to compete successfully with other solar cell technologies.[1−3] It is estimated[3] that the organic solar cells will become competitive with other thin film technologies only at efficiencies of more than 10% and the lifetimes more than 3−5 years. The low efficiency of organic solar cells is directly related to losses that occur at every step of the photogeneration, separation, and collection processes. However, there remains a considerable controversy concerning the mechanism of the recombination losses (geminate or nongeminate, bulk or interfacial) in organic solar cells.[4−20] It is widely considered that the main loss mechanism is the geminate recombination of the primary photoexcitons.[6,13−15,17,20,21] However, recent data[8,12,14] show that in photovoltaic blends with proper nanomorphology and phase segregation, the probability of fast exciton dissociation into free charge carriers approaches unity, and therefore other loss mechanisms need to be considered to further improve the efficiency of organic bulk heterojunction solar cells. One of these loss channels is interfacial recombination and poor charge extraction at the contacts. However, surprisingly, these processes have attracted little attention in the literature. Earlier this year, Street and Schoendorf published a paper[22] in which they suggested that the dominant recombination mechanism is through interfacial states at the polymer/PCBM (phenyl C_{60}−butyric acid methyl ester) interface. This finding was made on the basis of measurements of the intensity dependence of steady-state photocurrents, which prompted certain discussion[10,18] stemming from an assertion that a steady-state technique cannot unambiguously determine the loss mechanism. In this work, we study the mechanism of the recombination losses in poly(3-hexylthiohene) (P3HT):PCBM bulk heterojunction organic solar cells using two nonsteady-state techniques, namely, intensity modulated photocurrent spectroscopy (IMPS) and intensity modulated photovoltage spectroscopy (IMVS). We show that indeed one of the dominant loss mechanisms is nongeminate recombination via interfacial states. Furthermore, we demonstrate that the interfacial recombination is to a large extent responsible for the drastic loss in the cell efficiency upon aging.

A rapid deterioration of the photovoltaic performance of typical organic solar cells upon their aging is recognized as a very important issue that limits the competitiveness of organic solar cells.[3,23−27] While it is generally agreed that this deteriora-

Received: October 16, 2010
Accepted: January 5, 2011
Published: February 7, 2011

tion is due to incorporation of atmospheric oxygen and moisture into the active layer and recently a number of detailed studies,[26,27] including spatial and depth profiling of the physicochemical changes that occur upon aging[24,25] appeared in the literature, still there is insufficient knowledge of the specific degradation mechanisms and especially how aging affects various steps of the photocurrent generation and collection processes in organic solar cells.

IMPS and IMVS are well-known techniques that were successfully used in the past for the studies of the photoprocesses at various semiconductor electrodes[28−33,33−36] including organic single-layer or bilayer polymer solid-state solar cells[36,37] and are actively used at present for studies of dye-sensitized solar cells.[38−44] At the same time, we are aware of only one paper that describes an IMPS study of a bulk heterojunction organic solar cell,[45] which appeared when this manuscript was in preparation. However, the interpretation of the IMPS measurements in this paper was somewhat deficient. For instance, the analytical expression for the photocurrent obtained by Bag and Narayan[45] should result in the phase of the photocurrent staying negative at all frequencies, whereas the experimental data presented in this paper clearly showed a positive phase shift at low frequencies. To account for this, the authors introduced a certain effective parallel capacitance with an unclear physical meaning. Furthermore, Bag et al. interpreted their data in terms of primary exciton dissociation and recombination times, which are known to be in the nanosecond to picosecond range or even shorter[15] and thus can hardly be analyzed by IMPS measurements with the high frequency limit of 100 kHz as was done by Bag et al.[45]

The IMPS technique analyzes an ac photocurrent response of a photovoltaic system to intensity modulated illumination as a function of the modulation frequency. Since IMPS is a frequency domain technique, it is capable of characterizing the dynamic behavior of photovoltaic systems, as opposed to various dc methods like $I-V$ curve measurements/simulations. IMPS also offers distinct advantages over measurements of transient photocurrent/photovoltage/photoconductivity/time-of-flight/photo-CELIV (charge extraction by linearly increasing voltage) response to short illumination pulses since it allows one to separate the bulk (such as transport) and interfacial (such as surface recombination and charge extraction) processes. Furthermore, IMPS measurements are easier to relate to regular steady-state photocurrent measurements since they are essentially performed under normal working conditions of a solar cell, just using a modulated illumination. While IMPS cannot characterize the ultrafast processes related to primary photoexcitation and exciton dissociation, it is an excellent tool for studies of the transport and recombination processes as well as the processes of carrier recombination and extraction at the contacts. Furthermore, since IMPS uses a small ac harmonic perturbation, which can be easily superimposed onto a larger dc signal, IMPS offers a unique opportunity to investigate nonlinear behavior of photovoltaic systems with great accuracy.[31,32,40,46]

Toward this end, the IMPS response to such an ac + dc perturbation is analyzed as a function of both the modulation frequency of the ac component of the light intensity and the magnitude of the dc component. Since the ac perturbation is typically much smaller than the dc component, IMPS spectra represent a quasi-linear approximation, with the nonlinear behavior of the photovoltaic system manifesting itself through dependencies of the kinetic parameters of the photoprocess, as determined by IMPS, on the dc light intensity. In this work, this approach allowed us to separately evaluate the effect of the light intensity on different stages of the photoprocess. Specifically, it was found that the rate of the interfacial recombination of photoexcited electrons has two components, one of which increases linearly with the light intensity. This indicates that one of the dominant mechanisms of the recombination losses under these conditions is the interfacial recombination of electrons with photogenerated holes trapped at or near the interface. This finding was supported by Mott−Schottky measurements in the dark and under illumination that showed that the density of hole-occupied deep traps in the photovoltaic layer also increased with the light intensity.

2. EXPERIMENTAL SECTION

Materials and Device Fabrication. The solid state organic photovoltaic devices were prepared using a glass (1.1 mm)/ITO (100 nm)/PEDOT:PSS (70 nm)/P3HT:PCBM (90 nm)/Al (130 nm) architecture. Indium tin oxide (ITO) coated glass slides (Kintec, surface resistance < 10 ohm/□) were used as a transparent conducting anode. The ITO coated glass slides were cleaned by sonicating in a soap solution and rinsing multiple times with deionized water, followed by successive sonication for 20 min each in acetone, methanol, and isopropanol. The ITO slides were then activated by UV ozone treatment for 20 min prior to PEDOT:PSS deposition. PEDOT:PSS (Clevios PH1000 PEDOT grade, H.C. Stark) was filtered through a 1 μm glass filter to remove polymer aggregates, spin coated onto ITO coated glass slides in ambient conditions, and dried for 15 min at 95 °C. The samples were transferred to a glovebox with an inert Ar atmosphere (<1 ppm O_2 and H_2O). The photoactive layer consisted of a 1:1 mass ratio of P3HT (>95% regioregular, Solaris Chem) and PCBM (Solaris Chem) dissolved in dichlorobenzene and stirred overnight at 60 °C. The solution was filtered through a 0.45 μm PTFE filter to remove aggregates and spin coated onto the PEDOT:PSS layer. Samples were dried for 12 min at 90 °C and transferred without being exposed to ambient conditions under an inert Ar atmosphere to a vacuum chamber (base pressure < 4×10^{-6} Torr). Aluminum was deposited using thermal evaporation, and the completed devices were annealed at 150 °C for 11 min. Up to 5 cells were prepared from one PV slide by evaporating five independent Al electrodes. The bottom ITO glass electrode was also divided into five independent electrodes by selectively removing the conducting ITO layer between the cells. The geometric area of one cell was 0.26 cm^2. The cells were not encapsulated. After the fabrication, the cell efficiencies were evaluated using a Sciencetech solar simulator under the simulated AM1.5 solar light. Samples were stored under an inert Ar environment or in vacuum; however, they were briefly exposed to ambient conditions when they were loaded to the IMPS sample holder.

Measurement Procedures. For this work, we selected two representative cells that were prepared in identical conditions on the same photovoltaic slide. A number of other slides were also measured which generally produced similar results, with slight variations in the values of characteristic times, photocurrent magnitude, and other photovoltaic parameters. Two sets of measurements were performed, one a few days after the cell fabrication, and the other 2 months after the cell fabrication. All measurements were performed in an inert argon atmosphere using the aluminum electrode as a counter electrode and the ITO electrode as a working electrode. Cathodic photocurrents (electrons extracted at the Al electrode) were taken as having the positive sign in the IMPS plots. The IMPS measurements were performed under short-circuit conditions in the 1 MHz−1 Hz frequency range using a stand-alone Solartron 1260 frequency response analyzer. The light source was a 405 nm 20 mW laser diode (LD1510, Power Technology). The ac component of the light intensity was maintained constant at

8.0×10^{15} photons s^{-1} cm^{-2}, whereas the dc component increased stepwise from 8.2×10^{15} to 6.4×10^{16} photons s^{-1} cm^{-2} or from approximately 4 to 31 mW cm^{-2}. The chosen ac light intensity was shown in a separate experiment to be small enough to ensure the linear character of the cell response. The illuminated cell area was 0.03 cm^2. For the bias dependencies, IMPS spectra were acquired using a different setup that included a Solartron 1250 frequency response analyzer coupled with a PAR 263A potentiostat−galvanostat (Princeton Applied Research). Both setups were controlled by a version 2.8 ZPlot software (Scribner Associates Inc.). The IMVS spectra were acquired in open-circuit conditions in the 1 MHz−1 Hz frequency range using a stand-alone Solartron 1260 frequency response analyzer.

The Mott−Schottky measurements were performed in the dark and under the same dc light intensities as the IMPS measurements using a Solartron 1250 frequency response analyzer coupled with a PAR 263A potentiostat−galvanostat. The dc bias range was +0.6 V to −0.25 V. The amplitude of the ac voltage perturbation was 10 mV. A frequency of 6.626 kHz was used that was found high enough for the cells to be adequately represented by a serial RC circuit.

Procedures for Determination of Relaxation Time τ and the Exponent α. In the case of photocurrent relaxation at surface states with a single mean relaxation time, the IMPS photocurrent complex plane plots lay entirely within the first quadrant of the complex plane and can be described by the general equation of the form:[31,32,34,36,46]

$$j = g\left(1-\frac{\gamma}{1+(i\omega\tau)^{\alpha}}\right) \quad (1)$$

where g is the ac generation current (the flux of photogenerated carriers to the interface), τ is the characteristic relaxation time of the photogenerated carriers, γ is the fraction of carriers involved in the relaxation, ω is the angular light modulation frequency, and i is the imaginary unit. The exponent $0 \le \alpha \le 1$ is introduced to account for a distribution of relaxation times of the surface states, for instance, due to structural inhomogeneity or the fractal nature of the interface.[32] For an ideal interface with a single type of surface states, $\alpha = 1$ and the IMPS complex plane plot takes the shape of a semicircle. When α is less than unity, the center of the semicircle is located below the real axis resulting in the appearance of a depressed semicircle shape in the IMPS spectra.

The parameters γg, τ, and α can be determined by fitting the experimental frequency dependencies of the real and imaginary components Re(j) and Im(j) of the ac photocurrent using eq 1. Specifically, the following procedure was used:[32]

First, the experimental values of Re(j) and Im(j) were used to calculate the values of the function

$$Y = (j - \mathrm{Re}(j)_0)^{-1} \quad (2)$$

where $\mathrm{Re}(j)_0$ is the low-frequency limit of the ac photocurrent, $\mathrm{Re}(j)_0 = g(1-\gamma)$.

From eqs 1 and 2 one can obtain frequency dependencies of the real Re(Y) and imaginary Im(Y) components of function Y, as well as function Φ:

$$\mathrm{Re}(Y) = \frac{1}{\gamma g}\left(1+(\omega\tau)^{-\alpha}\cos\left(\frac{\alpha\pi}{2}\right)\right) \quad (3)$$

$$\mathrm{Im}(Y) = \frac{1}{\gamma g}(\omega\tau)^{-\alpha}\cos\left(\frac{\alpha\pi}{2}\right) \quad (4)$$

$$\Phi = \frac{\mathrm{Re}(Y)}{\mathrm{Im}(Y)}\,\mathrm{ctg}\left(\frac{\alpha\pi}{2}\right) = \frac{\omega^{\alpha}\tau^{\alpha}}{\sin\left(\frac{\alpha\pi}{2}\right)} \quad (5)$$

Then the exponent α can be found from the slope of the plot of $\ln(\mathrm{Im}(Y))$ vs $\ln(\omega)$ (see eq 4), and the relaxation time τ and thus the recombination rate constant $k = 1/\tau$ can be found from the slope of a linear plot of Φ versus ω^{α}. For the IMPS plots studied in this work, the values of the exponent α varied from 0.65 to 0.8, the average value being $\alpha = 0.75$. This is easily understood since the interfacial recombination most likely occurs at the bulk heterojunction interface between PCBM and P3HT phases (see below), which should feature a considerable fractal behavior as well as pronounced inhomogeneity.

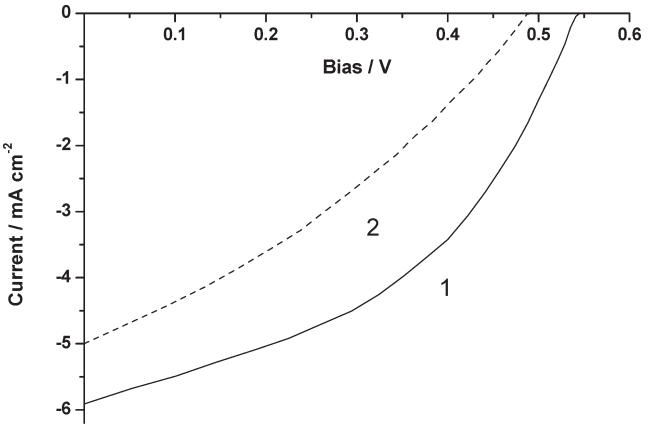

Figure 1. Experimental $I-V$ curves for two P3HT:PCBM cells after fabrication (plot 1, cell B; plot 2, cell A) prepared on the same photovoltaic slide.

The standard deviations σ and confidence intervals for parameters τ and k were determined from the same Φ,ω^{α} plots using the well-known equation for the standard deviations for the slope of a linear regression:

$$\sigma = \sqrt{\frac{\frac{1}{n-2}\sum_{i=1}^{n}\hat{\varepsilon}_i^2}{\sum_{i=1}^{n}(x_i-\bar{x})^2}} \quad (6)$$

where $\hat{\varepsilon}_i$ are the residuals of the linear model, n is the number of points, and $\bar{x}$ is the average value of the argument. The approximate 3 sigma rule was then used to determine the confidence intervals.

It should be noted that eqs 3−5 are valid only if the experimental IMPS plots correspond to relaxation at a single type of surface states. If the experimental frequency response of the photocurrent is distorted by the presence of additional relaxations such as carrier transport/recombination in the bulk or relaxation at more than one type of surface states, care should be taken to select the frequency range where the effects of these additional relaxations can be disregarded.

3. RESULTS AND DISCUSSION

In this work, we have been interested in the following goals:

(1) To analyze the ac photocurrent/photovoltage response of bulk-heterojunction P3HT:PCBM solar cells to intensity modulated illumination;
(2) To characterize using IMPS measurements at various dc light intensity levels the main mechanisms of recombination losses in the cells and separate the contributions of the bulk and interfacial processes;
(3) To gain insight into the changes in the carrier generation, separation, recombination, and extraction upon aging.

Shape of IMPS Response and the Correlation between IMPS Plots and Cell Efficiency. For this analysis we selected two cells that were prepared in identical conditions on the same photovoltaic slide but nevertheless featured a somewhat different

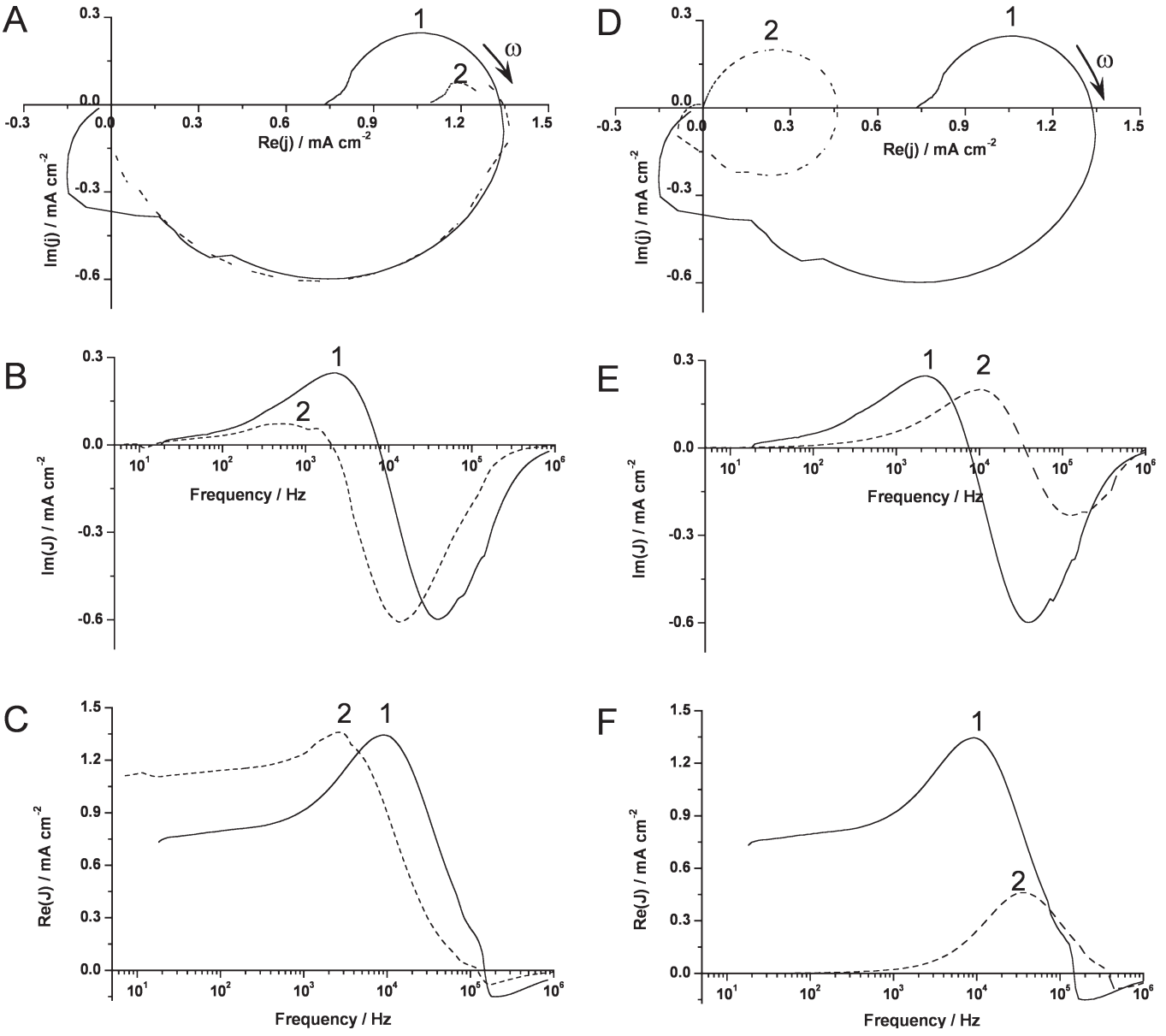

Figure 2. (A) Experimental IMPS spectra obtained at short-circuit conditions for two P3HT:PCBM photovoltaic cells (plot 1, cell A; plot 2, cell B) prepared on the same photovoltaic slide. (D) Comparison of experimental IMPS spectra for cell A (1) after fabrication and (2) after aging for 2 months. The arrows indicate the direction of increasing frequency. IMPS spectra are presented as Bode plots of (B, E) the imaginary and (C, F) the real components of the photocurrent response vs the modulation frequency. The dc light intensity for all spectra was 8.2×10^{15} s^{-1} cm^{-2}.

photovoltaic performance. Figure 1 presents the photocurrent−voltage curves for the two cells selected for this manuscript. Specifically (Figure 1), one of the cells that will be referred to as cell A showed V_{oc} of 0.51 V, I_{sc} of 5.00 mA cm^{-2}, and fill factor FF = 0.32, with the resulting power conversion efficiency of 0.82% (AM 1.5 simulated solar radiation immediately following cell fabrication). The other cell (cell B) showed a quite better efficiency of 1.4%, with V_{oc} of 0.55 V, I_{sc} of 5.91 mA cm^{-2}, and fill factor FF = 0.43. The goal was to understand the reasons for such a difference in performance and, specifically, whether it is related to variability in the properties of the photovoltaic layer, the contacts, or to some other factors.

Figure 2 shows the IMPS complex plane plots (A) and the corresponding Bode plots (B,C) obtained in identical conditions for cells A and B after their fabrication. The IMPS complex plane plots show similar shapes for the two cells, with the high-frequency regions located below the real axis in quadrants III and IV and the low-frequency arcs located above the real axis in quadrant I. The corresponding Bode plots of the imaginary component of the photocurrent (Figure 2B) show characteristic maxima and minima, which correspond to the maxima and minima of the two portions of the IMPS complex plane plot located in the I and IV quadrants, respectively. From Figure 2B one can estimate the characteristic relaxation times for the processes that correspond to the two portions of the plot. The high-frequency portions of the IMPS plots are similar to those observed with nanocrystalline systems[38−41] and can be related to the processes of carrier transport in the bulk of the photovoltaic layer. While there exists a fairly advanced understanding of these

processes in systems such as dye-sensitized solar cells, including the necessary mathematical analysis[35,38] the situation with organic photovoltaic systems is significantly different. Specifically, one needs to take into account the transport of excitons, holes, and electrons rather than electrons only; also, the assumption that there is no electric field in the semiconductor bulk that is customarily made with nanocrystalline systems may not hold here as well. At present, as far as we know, there is no mathematical analysis available in the literature that would allow adequate interpretation of the high-frequency portions of the IMPS responses under such circumstances, and it is likely that development of such analysis will take some time. The characteristic times of the high-frequency IMPS relaxation will therefore be interpreted broadly as a kind of carrier lifetime that should generally depend on the efficiency of carrier transport and extraction; however, at present, no further analysis of these phenomena is possible without an adequate mathematical analysis. The only fact we can note here is that this lifetime is shorter in less efficient cell A.

In the further discussion we concentrate on the low-frequency portions of the experimental IMPS response, which are located in the first quadrant of the complex plane. Importantly, as opposed to the IMPS response in nanocrystalline systems such as dye-sensitized solar cells where the IMPS response is largely determined by carrier transport and thus the photocurrent lags the light intensity, the photocurrent in this region leads the light intensity (both the real and the imaginary components are positive, thus producing a positive phase shift), and the photocurrent magnitude increases with the modulation frequency. Such behavior is hardly observed in nanoscrystalline solar cells and is a signature of the occurrence of interfacial recombination.[28−32,34,36] Furthermore, the fact that the photocurrent leads the light intensity suggests that the observed recombination is nongeminate. The photogenerated carriers first separate and charge the interface, which is seen as the growth of the photocurrent magnitude with a decrease in the modulation frequency in the high-frequency range; the interfacial recombination occurs only later (at lower frequencies) and involves the carriers that have already been separated and trapped at the surface/interfacial states. If the carriers were to remain bound or spatially correlated as in the case of geminate recombination, the separation of charges and the corresponding interfacial charging current would not be observed and the photocurrent would have lagged the light intensity and had a negative phase shift in the whole frequency range. Therefore, the fact that all experimental IMPS plots featured the low-frequency portions in quadrant I provides a direct evidence of the occurrence of nongeminate interfacial recombination in bulk heterojunction solar cells.

Furthermore, the IMPS results suggest that the interfacial recombination is a factor that to a large extent determines the cell efficiency. This can be seen by comparing the value of the ac photocurrent at the point at which the IMPS plot crosses the real axis from quadrant IV into quadrant I (often called the generation current) with the low-frequency limit of the photocurrent. The generation current indicates the maximum photocurrent that could be produced by a cell in the absence of interfacial recombination, whereas the low-frequency limit corresponds to the steady-state photocurrent that determines the actual cell conversion efficiency. From Figure 2 one can see that the photocurrent losses due to interfacial recombination can reach almost 50% in the case of the less efficient cell A. Furthermore, while the high-frequency portions of plots 1 and 2 of Figure 2A are nearly identical indicating that the bulk processes in these cells are very similar, it is the low-frequency portions due to interfacial recombination that determine the difference in the power conversion efficiencies between cells A and B. Furthermore, the frequency at the low-frequency maximum of the imaginary component of the photocurrent (Figure 2B) can be related to the rate of decay of photogenerated minority carriers at the surface states and in the first approximation can be considered equal to the pseudo-first-order rate constant k of the interfacial recombination[28−32,34,36] assuming that there is no carrier extraction through the interfacial states. As follows from the figure, the recombination rate constant is also higher for the less efficient cell A as compared to cell B. These facts suggest that the difference between these cells is not due to the bulk properties of the photovoltaic layer but rather is related to the processes at the contacts or at the interface between the donor and the acceptor components of the photovoltaic blend.

A similar conclusion of the importance of the interfacial recombination for the organic solar cell efficiency was reached recently by Street et al.[22,47] but on the basis of steady-state measurements. In this work, the use of IMPS allowed us to separate the bulk and the interfacial photoprocesses that occur in different frequency domains and obtain direct evidence that nongeminate interfacial recombination is an important loss mechanism.

IMPS Evidence of Increased Interfacial Recombination Rate in Aged Cells. Moreover, the interfacial recombination is more pronounced in aged cells. Figure 2D−F shows that while both the generation and the steady-state photocurrents decrease upon cell aging, the low-frequency portion in the IMPS plots is much more pronounced for the aged cell with the low-frequency intercept being close to zero. This correlates well with the regular photocurrent−voltage curves obtained for the aged cell under steady-state conditions using a solar simulator, which did not show any photocurrents whatsoever (the curves not presented). The frequency at the maxima of the low-frequency portions also increases with aging (Figure 2E) by about an order of magnitude indicating a considerable increase in the interfacial recombination rate. This means that interfacial recombination becomes a dominant loss mechanism in aged cells. At the same time, the high frequency portions of the photocurrent are greatly affected too: the photocurrent magnitude is smaller at virtually all frequencies and the frequency at the minimum of the high-frequency portion increases too indicating a shorter carrier lifetime in the bulk and presumably higher bulk recombination rate. All these facts suggest that aging affects all aspects of the operation of a solar cell; however, it should be pointed out that even aged cells would still be able to produce quite measurable photocurrent if not for the occurrence of interfacial recombination, as evidenced by the nonzero photocurrent values in the intermediate transitional region between the high and low frequency portions of the ac response. In other words, if the surface recombination could be suppressed, the aged cell efficiency would decrease significantly (perhaps, ca. 3 times as follows from Figure 2F) but still would not be zero. Again, this important conclusion could not be reached without IMPS allowing us to separate the bulk and interfacial processes through photocurrent analysis in the frequency domain.

IMPS and IMVS Responses at Varying dc Light Intensities. To gain a further insight into the mechanism of interfacial recombination, IMPS measurements at varying dc light intensities were performed (Figure 3). For a linear system, the ac IMPS response should not vary with the dc intensity; however, as follows from Figure 3, this is not the case. Specifically, the

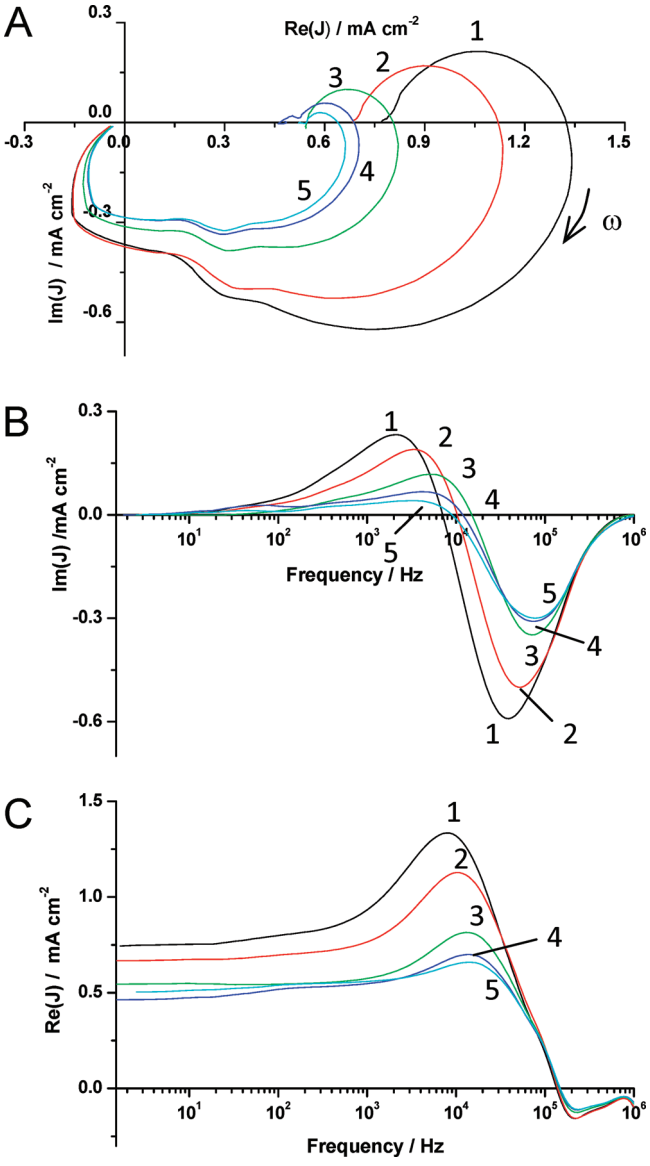

Figure 3. Intensity dependence of IMPS spectra measured at short-circuit conditions for photovoltaic cell A. The dc light intensities were (1) 8.2×10^{15} s^{-1} cm^{-2}; (2) 2.2×10^{16} s^{-1} cm^{-2}; (3) 3.5×10^{16} s^{-1} cm^{-2}; (4) 5.0×10^{16} s^{-1} cm^{-2}; and (5) 6.4×10^{16} s^{-1} cm^{-2}. The IMPS spectra are presented as (A) a Nyquist complex plane plot as well as Bode plots of (B) the imaginary and (C) the real components of the photocurrent response vs the modulation frequency. The arrow indicates the direction of increasing frequency.

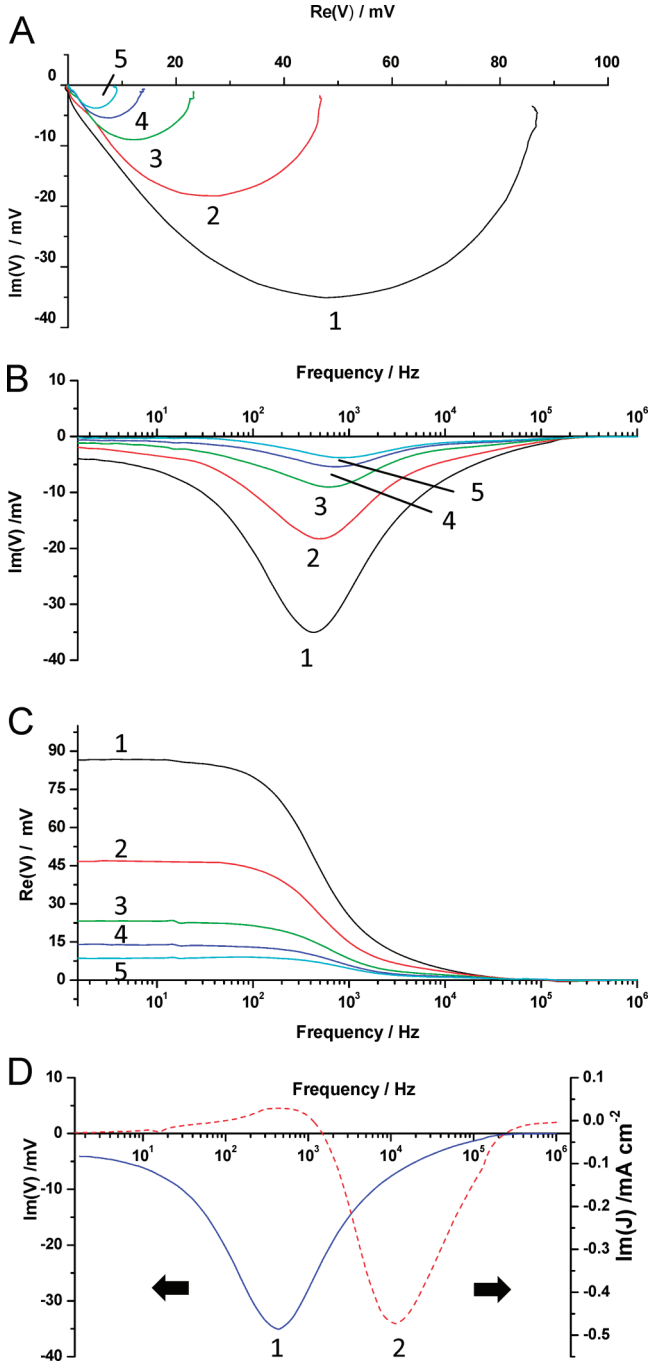

Figure 4. Intensity dependence of IMVS spectra measured at open-circuit conditions for photovoltaic cell A. The dc light intensities were (1) 8.2×10^{15} s^{-1} cm^{-2}; (2) 2.2×10^{16} s^{-1} cm^{-2}; (3) 3.5×10^{16} s^{-1} cm^{-2}; (4) 5.0×10^{16} s^{-1} cm^{-2}; and (5) 6.4×10^{16} s^{-1} cm^{-2}. The IMVS spectra are presented as (A) a Nyquist complex plane plot as well as Bode plots of (B) the imaginary and (C) the real components of the photovoltage response vs the modulation frequency. (D) Comparison of the frequency dependencies of the imaginary components of (1) IMVS photovoltage and (2) IMPS photocurrent response at a dc light intensity of 8.2×10^{15} s^{-1} cm^{-2}.

magnitude of the ac photocurrent, including its low-frequency limit that corresponds to the steady-state photocurrent, decreased with the light intensity, while the frequency at the extrema of the imaginary component of the photocurrent increased for both the high-frequency and low-frequency portions of the IMPS response (Figure 3B). In particular, there is a pronounced increase in the frequency at the maxima of the low frequency portions of the IMPS complex-plane plots, which indicates that increasing the dc light intensity increases the recombination rate constant *k*. It should be remembered that rate constant *k* is a pseudo-first-order rate constant that implicitly includes the population of the interfacial states with the majority carriers (holes in the case of P3HT). In linear systems it is independent of the light intensity since there is an excess of majority carriers at the interfacial states; however, if the surface state density or population can be modulated by light, the pseudo-first-order recombination rate constant will also have an intensity-dependent component.

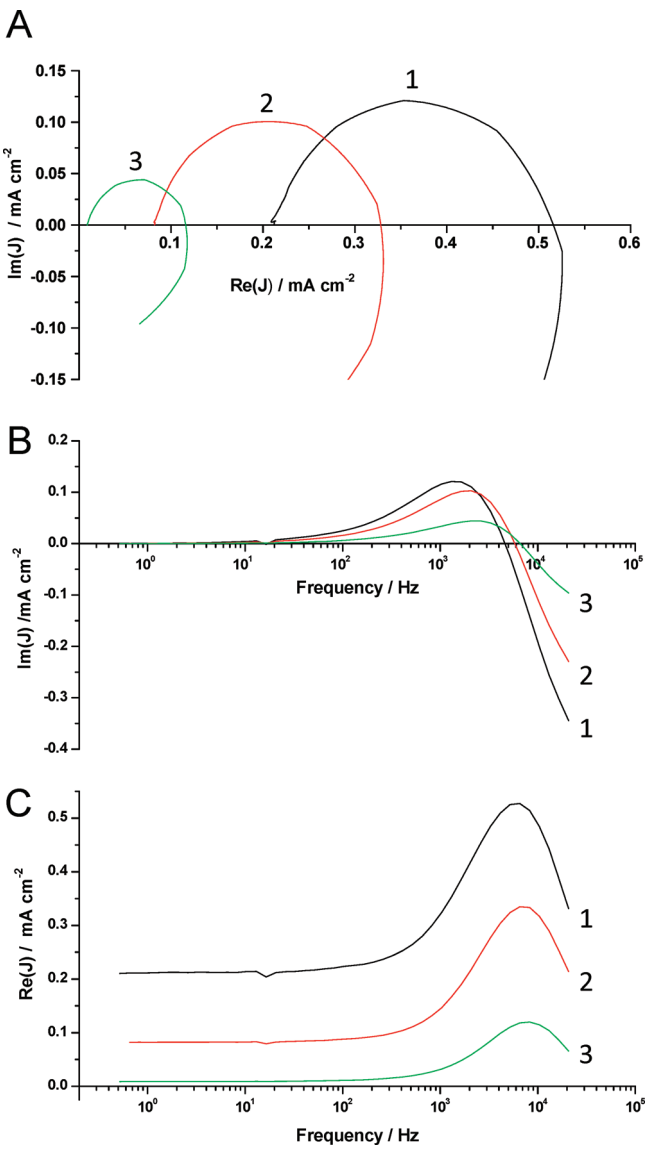

Figure 5. (A) Experimental IMPS spectra obtained at cell biases of 0.0 V (plot 1), +0.25 V (plot 2), and +0.5 V (plot 3) as well as Bode plots of (B) the imaginary and (C) the real components of the photocurrent response obtained at these bias values vs the modulation frequency.

Similar behavior is observed for the intensity modulated photovoltage (IMVS) response. Figure 4A−C shows the complex plane as well as Bode plots of the ac photovoltage measured for the photovoltaic cell A. It should be remembered that while IMPS spectra are measured at short-circuit conditions, IMVS spectra are measured at open circuit. Therefore, there is no carrier extraction and IMVS spectra just show accumulation of charge at the interface. Then the characteristic frequency at the minimum of the imaginary component of the photovoltage can be in the first approximation taken as the lifetime of carriers at the surface states,[40] which is the inverse of the pseudo-first-order recombination rate constant at open circuit. Figure 4 again suggests, now on the basis of IMVS data, that the recombination rate constant k increases with the light intensity. Furthermore, as follows from Figure 4D, the frequencies at maxima and thus the lifetimes of carriers at the interfacial states derived from IMPS and IMVS data are quite close. This may suggest, among other facts, that there is no extraction of photogenerated carriers through the interfacial states (the lifetime is determined by the recombination rate only). If there were noticeable carrier extraction through the surface states, then the characteristic relaxation times derived from IMPS and IMVS spectra would have been quite different (IMPS is measured when carriers are extracted giving rise to photocurrent and IMVS is measured at open circuit when no extraction is possible). At the same time, this conclusion needs further justification, especially given the fact that the recombination constant is bias-dependent (see below) and IMPS and IMVS are measured at different bias values. However, the IMVS data unambiguously suggest that it is the recombination rate and not the rate of the carrier extraction that increases with the light intensity since no carrier extraction is possible in these conditions.

Bias Dependence of IMPS Response. Figure 5 shows the evolution of IMPS spectra under applied bias. It should be noted that these data had to be obtained with a different setup that included a potentiostat, which reduced the bandwidth and affected the measurement frequency range. Nevertheless, one can clearly see that the recombination rate constant increased when the bias was changed from short-circuit (E = 0.0 V) to near open-circuit conditions (E = +0.5 V). This indicated that the population of the interfacial states or their density is not only intensity- but also bias-dependent. The photocurrent magnitude also decreased, as could be expected in view of the bias dependence of the photocurrent (Figure 1). While a decrease in the photocurrent alone could be attributed to a lower probability of exciton dissociation with a decrease in the electric field, this mechanism cannot explain the corresponding changes in the interfacial recombination rate revealed by IMPS. This again highlights the importance of interfacial recombination as a major loss channel. Moreover, the increase in the recombination rate near the open circuit should have a detrimental effect on the cell fill factor and further reduce the efficiency.

Mott−Schottky Measurements in the Dark and under Illumination. To find an explanation for the observed light intensity dependence of the recombination rate constant k, dependencies of the cell capacitance C on the applied bias E were measured in the dark and under illumination. The corresponding C^{-2}, E plots for cell A in the dark and for a series of dc light intensities are presented in Figure 6. If a C^{-2}, E (Mott−Schottky) plot is linear, this indicates that there is a space charge region in the semiconductor near the contact, which is set up by ionized donor or acceptor species and the width of which increases as the square root of the applied bias. The Mott−Schottky behavior may occur within a limited bias range only due to potential drop redistribution or other factors such as a finite semiconductor layer thickness. The slope of the linear portions of Mott−Schottky plots is inversely proportional to the dopant density in the films.[48] For a p-type conjugated polymer semiconductor, the dopant density does not represent dopant ions but instead is due to positively charged polarons/bipolarons in the film.[49,50] Such polarons/bipolarons may form due to trapping of photoexcited holes at certain portions of the polymer backbone or, for instance, oxygen-induced doping.[27]

As follows from Figure 6, the experimental Mott−Schottky plots all had linear portions at more negative bias values, in agreement with the literature data[26,49,50] and the anticipated p-type semiconductor behavior. Furthermore, the slopes of the Mott−Schottky plots decreased with the light intensity. This indicates that illumination results in an increase in the density of

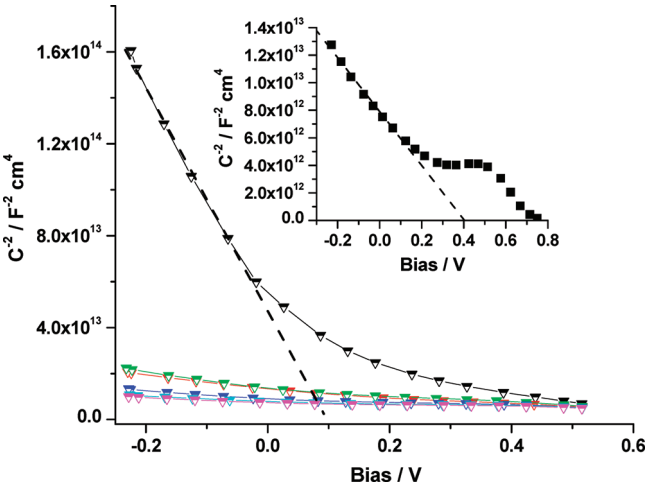

Figure 6. Mott−Schottky plots for photovoltaic cell A measured in the dark (plot 1) and as a function of the dc light intensity (plots 2−6). The light intensity values were (2) 8.2×10^{15} s^{-1} cm^{-2}; (3) 2.2×10^{16} s^{-1} cm^{-2}; (4) 3.5×10^{16} s^{-1} cm^{-2}; (5) 5.0×10^{16} s^{-1} cm^{-2}; and (6) 6.4×10^{16} s^{-1} cm^{-2}. The inset shows an enlarged Mott−Schottky plot at a dc light intensity of 5.0×10^{16} s^{-1} cm^{-2}.

trapped holes near the interface. Similar changes in the slope of Mott−Schottky plots due to illumination were recently observed in the literature.[26] Indeed, charge trapping is known to occur in such relatively disordered media as organic semiconducting polymers.[51,52] Furthermore, illumination changes the shape of the C^{-2}, E dependencies. As seen in the inset in Figure 6, under illumination the decrease in the C^{-2} values with the applied bias is interrupted from approximately 0.2 V to approximately 0.5 V, and the Mott−Schottky plot shows a plateau. The occurrence of such a plateau is usually attributed to the Fermi level pinning by the interfacial states. When a Fermi level passes through a set of interfacial states with a relatively high density, the applied bias will be localized at the capacitance of these states, and there will be little or no change in the potential drop in the space charge region and correspondingly little change in its capacitance. The Fermi level will stay pinned to the interfacial states until all such states are charged or discharged. Therefore, the occurrence of the Fermi level pinning under illumination indicates formation of a large density of interfacial states under illumination. Such midgap states formation was observed by Schafferhans et al. in P3HT:PCBM blends under illumination using a thermally stimulated current technique.[27] They also found that such states had their activation energy within a range from 0.2 to 0.4 eV, which agrees quite well with our data (inset in Figure 6).

Correlation between the Interfacial Recombination Rate and the Charged Trap Density. Therefore, it was found that illumination facilitates trapping of photogenerated holes at and near the P3HT:PCBM interface. These holes may be able to participate in recombination with photogenerated electrons, which could be the reason of the nonlinear photocurrent and photovoltage response and the experimentally observed increase in the apparent pseudo-first-order recombination constant with the light intensity. To support this line of reasoning, we looked into the dependencies of the recombination constant k and the charged trap density N_D on the light intensity. Such data are given in Figure 7.

The values of k in Figure 7 were determined by fitting the frequency dependencies of the real and imaginary components of

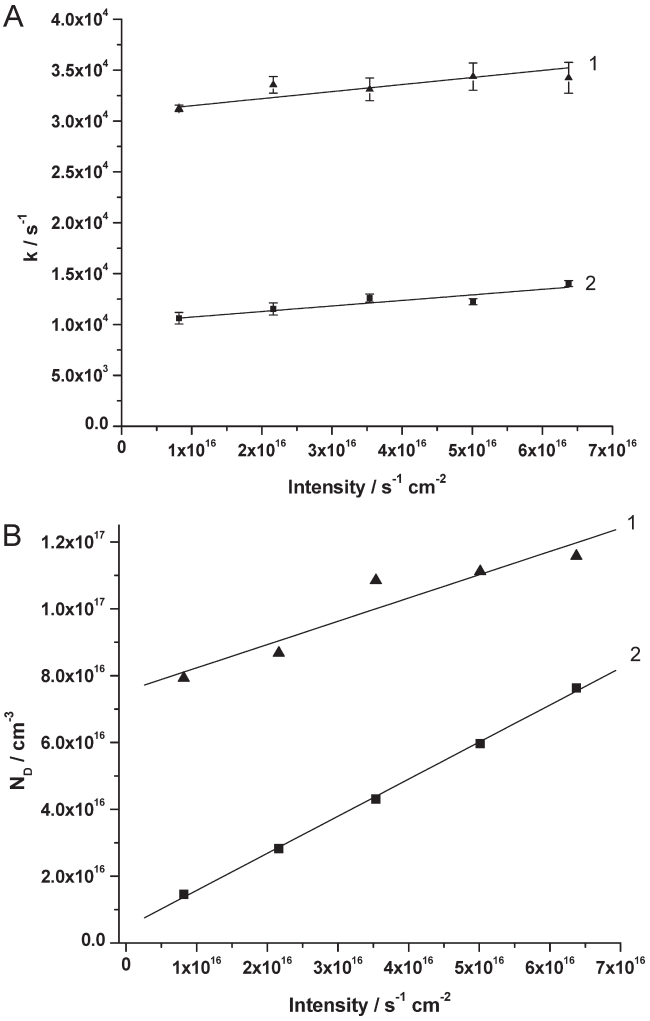

Figure 7. Dependencies on the dc light intensity of (A) interfacial recombination rate constant derived from the IMPS plots and (B) trap density obtained from the Mott−Schottky plots for photovoltaic cell A. For each graph, plot 1 corresponds to the photovoltaic cell after aging for 2 months and plot 2 corresponds to a photovoltaic cell after fabrication.

the photocurrent as described in the Experimental Section. The corresponding dependencies of k vs dc light intensity for the two cells under study are shown in Figure 7A. One can see that both cell types showed a linear increase in the recombination rate with the dc intensity. At the same time, the values of k extrapolated to zero dc intensity were not zero. This means that the interfacial recombination rate has two components, one of which is dependent and the other independent of the light intensity. The k values were higher for the aged cell, as could be expected.

Similar dependencies were found for the trapped holes density N_D. Figure 7B presents the dependencies of the trap density on the dc light intensity for cell A after fabrication (plot 2) and after aging (plot 1). Again, N_D values were found to scale linearly with the light intensity. Furthermore, the dependencies again showed nonzero intercepts at zero dc light intensity, which was especially pronounced in the aged cell. This means that the trap density, like the recombination constant, has two components, one dependent and another independent of the light intensity. Furthermore, one can see that the trap density is much higher in the aged cell even in the dark, which may be another factor

responsible for the increase in the interfacial recombination rate upon aging.

Localization of the Interfacial States. An organic bulk heterojunction solar cell is a complex device that contains many interfaces. Therefore, it is important to determine the localization of the interfacial states that are responsible for the observed recombination losses to be able to further improve the cell efficiency. In our opinion, the most likely location of the interfacial states responsible for recombination evidenced by the IMPS and IMVS data is the interface between the PCBM and the P3HT phases. The reason is that it is the interface at which the separation of the primary photoexcitons occurs and at which the electrons are transferred into the PCBM phase. Furthermore, efficient cells are vertically organized in such a way that the majority of the PCBM phase is located closer to the top metal contact. For an electron to recombine at the ITO/PEDOT or PEDOT/P3HT:PCMB interfaces, it would have to transfer back into the P3HT phase and travel across the photovoltaic layer, which seems unlikely. It is possible that some electrons that are photogenerated in the P3HT phase without the use of the donor−acceptor mechanism may recombine at these interfaces, as was demonstrated for single layer polymer solar cell without the acceptor component,[36] but the photocurrents in this case are very small and cannot account for the relaxations seen in Figures 2−4.

The recombination cannot happen at the Al/PCBM interface as well because PCBM forms an Ohmic contact with Al;[53,54] furthermore, there should be no holes in the PCBM phase. The only other possible location would be the portions of the Al contact where the metal is in direct contact with P3HT. Such locations are essentially defects, but they are found in bulk heterojunction cells. Then the recombination could occur at the Al/P3HT interface with PCBM clusters located in the close proximity or with electrons provided through the metal contact. Further studies are required to investigate this possibility, for instance, by introducing barrier interfacial layers such as LiF.

The conclusion about the most likely localization of the interfacial states is also supported by the results with the aged cells. The increase in the interfacial recombination rate can be attributed to an increase in the density of states at the interface, as well as increased charge trapping near the interface upon aging. Both these processes are likely to be related to chemical and structural changes induced by illumination in the presence of oxygen and moisture.[24−27] The specific mechanisms involved in these processes are yet to be fully understood. However, recent measurements of the distribution of the oxygen and water intake in bulk heterojunction cells during their degradation[24] show a considerable accumulation of oxygen at the Al/P3HT:PCBM interface (the resolution of the mapping in this study was not high enough to distinguish between P3HT and PCBM components of the photovoltaic layer).

4. CONCLUSIONS

1. The IMPS and IMVS measurements in the frequency domain allowed us to separate the contribution of the bulk and interfacial processes and provide direct evidence of the occurrence of nongeminate recombination through interfacial states. This recombination appears to be a major loss mechanism, especially, in aged cells. While the geminate recombination of primary excitons remains an important process, especially in photovoltaic films with poor morphology and phase separation, the latest data suggest that almost all primary excitons in the best photovoltaic cells give rise to free carriers, and then the recombination losses through interfacial states analyzed here become especially important as an untapped resource for further efficiency improvements.
2. The interfacial recombination shows a mixture of the first-order and second-order kinetics. The reason for the latter process exhibited through nonlinear dependence of the photocurrent on the light intensity is the trapping of photoexcited holes in P3HT phase at and near the interface with PCBM and/or Al.
3. The interfacial recombination centers are located either at the P3HT:PCBM internal heterojunction interface or at the Al contact with the photovoltaic layer with both P3HT and PCBM domains being in close proximity to the contact. Further studies are needed to clarify this point, for instance, using modification of the contacts with various sublayers such as LiF. However, the most likely location of the interfacial states responsible for the recombination is at the interface between the PCBM and the P3HT phases. In this case, the increase in the interfacial recombination rate may be due to nanoscale structural changes and specifically changes in the phase segregation in the P3HT:PCBM layer upon aging. Further studies of these processes are required.
4. The rate of the interfacial recombination greatly increases with aging to the point that it effectively controls the efficiency of aged cells. This fact may be related to formation of recombination centers facilitated by oxygen/water intake and illumination.
5. Our findings enable us to make the following recommendations concerning the ways to further improve the efficiency of bulk heterojunction organic solar cells:

   (i) Reduce trapping of charges in the photovoltaic layer. The means may be better morphological control, improving mobilities, and so forth.
   (ii) Reduce the density of interfacial states at the interface. Possible means may include strict control of exposure to oxygen and water, as well as surface modification.
   (iii) Improve the carrier extraction efficiency at contacts. If the rate of charge extraction is high enough, it should be able to compete efficiently with carrier capture by the interfacial states and interfacial recombination. Our results indicate that the typical relaxation times at the interfacial states are 0.1−1 ms, which means that the cross-section of the electron capture by the interfacial states cannot be very high. This recommendation is not new, but it gains new significance in view of our results showing the importance and the extent of recombination losses at the interfaces.
6. IMPS and IMVS techniques show significant potential for studies of the mechanism of photocurrent generation and recombination losses in organic solar cells in the intermediate time/frequency range. With the recent research efforts resulting in drastic improvements of the charge separation processes on the ultrafast time scale, the losses due to slow transport, poor carrier extraction, and interfacial recombination should become the primary targets to further improve the efficiency of bulk heterojunction organic solar cells.

AUTHOR INFORMATION

Corresponding Author

*E-mail: osemenik@uwo.ca. Phone: +1 519 661 2111, ext. 82858. Fax: +1 519 661 3022.

ACKNOWLEDGMENT

The support by the Natural Sciences and Engineering Research Council of Canada (NSERC) and especially its Engage program, Canada Foundation for Innovation/Ontario Innovation Trust (CFI/OIT), as well as the Academic Development Fund of the University of Western Ontario is gratefully acknowledged.

REFERENCES

(1) Dennler, G.; Scharber, M. C.; Brabec, C. J. *Adv. Mater.* **2009**, *21*, 1323–1338.
(2) Deibel, C.; Dyakonov, V. *Rep. Prog. Phys.* **2010**, *73*, 096401.
(3) Nielsen, T. D.; Cruickshank, C.; Foged, S.; Thorsen, J.; Krebs, F. C. *Sol. Energy Mater. Sol. Cells* **2010**, *94*, 1553–1571.
(4) Pivrikas, A.; Juska, G.; Mozer, A. J.; Scharber, M.; Arlauskas, K.; Sariciftci, N. S.; Stubb, H.; Osterbacka, R. *Phys. Rev. Lett.* **2005**, *94*, 176806.
(5) Koster, L. J. A.; Smits, E. C. P.; Mihailetchi, V. D.; Blom, P. W. M. *Phys. Rev. B: Condens. Matter Mater. Phys.* **2005**, *72*, 085205.
(6) Koster, L. J. A.; Mihailetchi, V. D.; Blom, P. W. M. *Appl. Phys. Lett.* **2006**, *88*, 052104.
(7) Deibel, C.; Wagenpfahl, A.; Dyakonov, V. *Phys. Rev. B: Condens. Matter Mater. Phys.* **2009**, *80*, 075203.
(8) Bakulin, A. A.; Hummelen, J. C.; Pshenichnikov, M. S.; van Loosdrecht, P. H. M. *Adv. Funct. Mater.* **2010**, *20*, 1653–1660.
(9) Collins, B. A.; Gann, E.; Guignard, L.; He, X.; McNeill, C. R.; Ade, H. *J. Phys. Chem. Lett.* **2010**, *1*, 3160–3166.
(10) Deibel, C.; Wagenpfahl, A. *Phys. Rev. B: Condens. Matter Mater. Phys.* **2010**, *82*, 207301.
(11) Deibel, C.; Strobel, T.; Dyakonov, V. *Adv. Mater.* **2010**, *22*, 4097–4111.
(12) Guo, J. M.; Ohkita, H.; Benten, H.; Ito, S. *J. Am. Chem. Soc.* **2010**, *132*, 6154–6164.
(13) Hamilton, R.; Shuttle, C. G.; O'Regan, B.; Hammant, T. C.; Nelson, J.; Durrant, J. R. *J. Phys. Chem. Lett.* **2010**, *1*, 1432–1436.
(14) Howard, I. A.; Mauer, R.; Meister, M.; Laquai, F. *J. Am. Chem. Soc.* **2010**, *132*, 14866–14876.
(15) Howard, I. A.; Laquai, F. *Macromol. Chem. Phys.* **2010**, *211*, 2063–2070.
(16) Shoaee, S.; Eng, M. P.; Espildora, E.; Delgado, J. L.; Campo, B.; Martin, N.; Vanderzande, D.; Durrant, J. R. *Energy Environ. Sci.* **2010**, *3*, 971–976.
(17) Shuttle, C. G.; Hamilton, R.; O'Regan, B. C.; Nelson, J.; Durrant, J. R. *Proc. Natl. Acad. Sci. U.S.A.* **2010**, *107*, 16448–16452.
(18) Street, R. A. *Phys. Rev. B: Condens. Matter Mater. Phys.* **2010**, *82*, 207302.
(19) Hilczer, M.; Tachiya, M. *J. Phys. Chem. C* **2010**, *114*, 6808–6813.
(20) Clarke, T. M.; Ballantyne, A. M.; Shoaee, S.; Soon, Y. W.; Duffy, W.; Heeney, M.; McCulloch, I.; Nelson, J.; Durrant, J. R. *Adv. Mater.* **2010**, *22*, 5287–5291.
(21) Shuttle, C. G.; O'Regan, B.; Ballantyne, A. M.; Nelson, J.; Bradley, D. D. C.; Durrant, J. R. *Phys. Rev. B: Condens. Matter Mater. Phys.* **2008**, *78*, 113201.
(22) Street, R. A.; Schoendorf, M. *Phys. Rev. B: Condens. Matter Mater. Phys.* **2010**, *81*, 205307.
(23) Jorgensen, M.; Norrman, K.; Krebs, F. C. *Sol. Energy Mater. Sol. Cells* **2008**, *92*, 686–714.
(24) Norrman, K.; Gevorgyan, S. A.; Krebs, F. C. *ACS Appl. Mater. Interfaces* **2009**, *1*, 102–112.
(25) Norrman, K.; Madsen, M. V.; Gevorgyan, S. A.; Krebs, F. C. *J. Am. Chem. Soc.* **2010**, *132*, 16883–16892.
(26) Seemann, A.; Sauermann, T.; Lungenschmied, C.; Armbruster, O.; Bauer, S.; Egelhaaf, H. J.; Hauch, J. *Sol. Energy* **2010**, doi: 10.106/j.solener.2010.09.007.
(27) Schafferhans, J.; Baumann, A.; Wagenpfahl, A.; Deibel, C.; Dyakonov, V. *Org. Electron.* **2010**, *11*, 1693–1700.
(28) Li, J.; Peter, L. M. *J. Electroanal. Chem.* **1985**, *193*, 27–47.
(29) Li, J.; Peter, L. M. *J. Electroanal. Chem.* **1986**, *199*, 1–26.
(30) Peter, L. M. *Chem. Rev.* **1990**, *90*, 753–769.
(31) Rotenberg, Z. A.; Semenikhin, O. A. *J. Electroanal. Chem.* **1991**, *316*, 165–174.
(32) Semenikhin, O. A.; Rotenberg, Z. A. *Sov. Electrochem.* **1992**, *28*, 992–999.
(33) de Jongh, P. E.; Vanmaekelbergh, D. *J. Phys. Chem. B* **1997**, *101*, 2716–2722.
(34) Semenikhin, O. A.; Kazarinov, V. E.; Jiang, L.; Hashimoto, K.; Fujishima, A. *Langmuir* **1999**, *15*, 3731–3737.
(35) Vanmaekelbergh, D.; de Jongh, P. E. *Phys. Rev. B: Condens. Matter Mater. Phys.* **2000**, *61*, 4699–4704.
(36) DiCarmine, P. M.; Semenikhin, O. A. *Electrochim. Acta* **2008**, *53*, 3744–3754.
(37) Manoj, A. G.; Alagiriswamy, A. A.; Narayan, K. S. *J. Appl. Phys.* **2003**, *94*, 4088–4095.
(38) Dloczik, L.; Ileperuma, O.; Lauermann, I.; Peter, L. M.; Ponomarev, E. A.; Redmond, G.; Shaw, N. J.; Uhlendorf, I. *J. Phys. Chem. B* **1997**, *101*, 10281–10289.
(39) Peter, L. M.; Ponomarev, E. A.; Franco, G.; Shaw, N. J. *Electrochim. Acta* **1999**, *45*, 549–560.
(40) Kruger, J.; Plass, R.; Gratzel, M.; Cameron, P. J.; Peter, L. M. *J. Phys. Chem. B* **2003**, *107*, 7536–7539.
(41) Dunn, H. K.; Peter, L. M. *J. Phys. Chem. C* **2009**, *113*, 4726–4731.
(42) Schlichthorl, G.; Huang, S. Y.; Sprague, J.; Frank, A. J. *J. Phys. Chem. B* **1997**, *101*, 8141–8155.
(43) Zhu, K.; Neale, N. R.; Miedaner, A.; Frank, A. J. *Nano Lett.* **2007**, *7*, 69–74.
(44) Zhu, K.; Neale, N. R.; Halverson, A. F.; Kim, J. Y.; Frank, A. J. *J. Phys. Chem. C* **2010**, *114*, 13433–13441.
(45) Bag, M.; Narayan, K. S. *Phys. Rev. B: Condens. Matter Mater. Phys.* **2010**, *82*, 075308.
(46) Rotenberg, Z. A. *Sov. Electrochem.* **1992**, *28*, 1307–1311.
(47) Street, R. A.; Cowan, S.; Heeger, A. J. *Phys. Rev. B: Condens. Matter Mater. Phys.* **2010**, *82*, 121301.
(48) Bard, A. J.; Memming, R.; Miller, B. *Pure Appl. Chem.* **1991**, *63*, 569–596.
(49) Semenikhin, O. A.; Ovsyannikova, E. V.; Alpatova, N. M.; Rotenberg, Z. A. *J. Electroanal. Chem.* **1996**, *408*, 67–75.
(50) Semenikhin, O. A.; Hossain, M. M. D.; Workentin, M. S. *J. Phys. Chem. B* **2006**, *110*, 20189–20196.
(51) Blom, P. W. M.; Vissenberg, M. C. J. M. *Mater. Sci. Eng., R* **2000**, *27*, 53–94.
(52) Chiguvare, Z.; Dyakonov, V. *Phys. Rev. B: Condens. Matter Mater. Phys.* **2004**, *70*, 235207.
(53) Mihailetchi, V. D.; van Duren, J. K. J.; Blom, P. W. M.; Hummelen, J. C.; Janssen, R. A. J.; Kroon, J. M.; Rispens, M. T.; Verhees, W. J. H.; Wienk, M. M. *Adv. Funct. Mater.* **2003**, *13*, 43–46.
(54) Mihailetchi, V. D.; Blom, P. W. M.; Hummelen, J. C.; Rispens, M. T. *J. Appl. Phys.* **2003**, *94*, 6849–6854.